Journal of Alloys and Compounds 501 (2010) 265–268

Contents lists available at ScienceDirect

Journal of Alloys and Compounds

journal homepage: www.elsevier.com/locate/jallcom

Hydrothermal synthesis of Co-doped ZnO flakes with room temperature ferromagnetism

Xingyan Xu, Chuanbao Cao*

Research Center of Materials Science, Department of Materials Science & Engineering, Beijing Institute of Technology, Beijing 100081, China

ARTICLE INFO

Article history:
Received 26 October 2009
Received in revised form 13 April 2010
Accepted 14 April 2010
Available online 22 April 2010

Keywords:
Diluted magnetic semiconductor
Co-doped ZnO flakes
Room temperature ferromagnetism

ABSTRACT

A series of high quality $Zn_{1-x}Co_xO$ ($x \leq 0.10$) flakes were synthesized by hydrothermal route. XRD and TEM characterizations indicate that the as-prepared samples were crystalline with wurtzite structure and no metallic Co or other secondary phases were found. Optical absorption and Raman results further confirm the incorporation of Co^{2+} ions in the ZnO lattice. Magnetic measurements indicate that the $Zn_{1-x}Co_xO$ ($x \leq 0.1$) flakes show obvious ferromagnetic characteristics at room temperature. However, at higher doping content of Co^{2+}, the ferromagnetic behavior was suppressed and paramagnetic nature was observed. The decrease of ferromagnetism with increasing doping concentration demonstrates that ferromagnetism observed at room temperature is an intrinsic property of $Zn_{1-x}Co_xO$ flakes, and does not originate from any secondary phase.

1. Introduction

Diluted magnetic semiconductors (DMS) that are formed by the partial replacement of cations in semiconductors by magnetic transition-metal ions have drawn considerable attention because of their potential for use in future spintronic devices [1,2]. The main challenge for practical applications of the DMS materials is the attainment of ferromagnetism (FM) above room temperature (RT). Recently, transition-metal-doped ZnO DMS have been extensively investigated since theoretical studies predicted their Curie temperature (T_C) to be above room temperature [3]. Moreover, ZnO has broadband gap, and possesses a large exciton binding energy of 60 meV and UV lasing properties at room temperature. Combining the excellent optical properties with room temperature ferromagnetism, many magneto-optic devices could be made from ZnO-based DMS. However, experimental observations of magnetism of the Co-doped ZnO synthesized by different methods have been controversial for both thin films and bulk samples. A number of groups observed no ferromagnetism in $Zn_{1-x}Co_xO$ [4–6], while Kalyana Lakshmi et al. [7] and Maensiri et al. [8] reported ferromagnetism in Co-doped ZnO powders. Kittilstved et al. [9] and Rubi et al. [10] demonstrated that ferromagnetism of n-type $Zn_{1-x}Co_xO$ thin films and powders could be switched on or off by chemical manipulation using nitrogen or oxygen, respectively. Qiu et al. [11] reported room temperature ferromagnetism (RTFM) of Co-doped ZnO prepared by a novel water-bubble template process. The origin of the observed FM in these samples is still debated. While many reports support the intrinsic mechanisms such as carrier-mediated ferromagnetism [12] and bound magnetic polaron (BMP) model [13], Co-metal clustering in $Zn_{1-x}Co_xO$ powders was argued to be responsible for the observed ferromagnetism [14,15]. It is therefore imperative to fabricate Co-doped ZnO under suitable conditions that diminish the extrinsic uncertainties and study the influence of doping concentration on ferromagnetism, and then effectively clarify the intrinsic origin of ferromagnetism.

In this paper, we report the synthesis of high quality $Zn_{1-x}Co_xO$ flakes by hydrothermal route and investigate the doping concentration dependence of ferromagnetism.

2. Experimental

Highly crystalline $Zn_{1-x}Co_xO$ ($x \leq 0.15$) flakes have been prepared by hydrothermal route. 2 mmol zinc nitrate ($Zn(NO_3)_2{\cdot}6H_2O$) and the required amount of cobalt nitrate ($Co(NO_3)_2{\cdot}6H_2O$) were dissolved in de-ionized water to form a 40 ml solution. Certain amount of urea was introduced into the above solution under magnetic stirring and the contents were transferred to a teflon-lined stainless steel autoclave of 50 ml capacity and kept at 180 °C for 10 h. After the reaction, the products were collected and thoroughly washed with distilled water and ethanol, and finally dried at 120 °C for 10 h in vacuum. The series of $Zn_{1-x}Co_xO$ flakes, light green in colour, become darker with increasing Co content. The powders were characterized by X-ray diffraction analysis (XRD, X' Pert Pro MPD) with CuKα radiation ($\lambda = 0.15406$ nm). The morphology of the products was observed by scanning electron microscopy (SEM), using a Hitachi TM-1000 scanning electron microanalyzer and transmission electron microscope (TEM) equipped with selected area electron diffraction (SAED) (Hitachi H-800 transmission electron microscope with a tungsten filament and an accelerating voltage of 200 kV). The optical absorption spectra were measured in the range 200–800 nm using a UV–vis absorption spectrometer (U-4100, Hitachi). Micro-Raman scattering experiments were done using a micro-Raman spectrometer with the 514.5 nm line of an Ar^+ laser as excitation source (JY-T64000, France).

* Corresponding author. Tel.: +86 10 68913792; fax: +86 10 68913937.
E-mail address: cbcao@bit.edu.cn (C. Cao).

0925-8388/$ – see front matter © 2010 Elsevier B.V. All rights reserved.
doi:10.1016/j.jallcom.2010.04.086

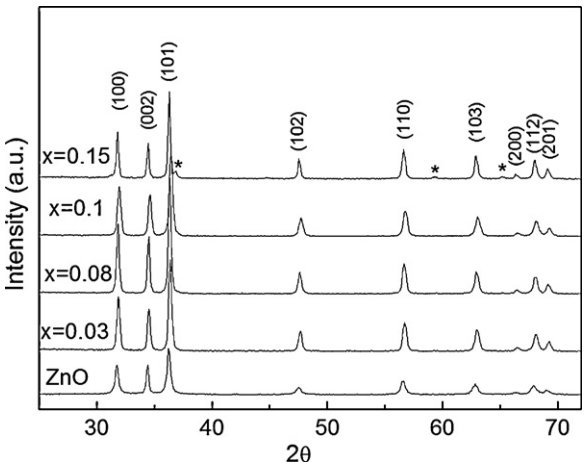

Fig. 1. X-ray diffraction patterns of $Zn_{1-x}Co_xO$ flakes ($x \leq 0.15$).

Magnetic measurements were done using Lake Shore 7300 vibrating sample magnetometer (VSM) at room temperature.

3. Results and discussion

The XRD patterns of different $Zn_{1-x}Co_xO$ ($x \leq 0.15$) flakes are shown in Fig. 1. These XRD patterns show that no other impurity phases exist for doping concentration below $x = 0.1$. The Co-doping does not change the wurtzite structure of ZnO. With increasing Co-doping concentration to 0.15, the diffraction pattern displays a weak undesired peak of Co_3O_4 (labeled by *). The lattice parameters calculated from the XRD data demonstrate that their values are close to but slightly smaller than those of pure ZnO (see Table 1). In addition, it is noticeable that the variation of the lattice parameters with Co concentration is not monotonic. The above results are understandable, because the effective ionic radius (0.58 Å) of Co in tetrahedral configuration is close to that of Zn^{2+} (060 Å) [16,17].

The SEM and TEM images corresponding to the sample $Zn_{0.9}Co_{0.1}O$ are shown in Fig. 2. As shown in Fig. 2a, large quantities of flake structures are observed. The TEM image shows the surface of the flake to be porous and rough (Fig. 2b). The corresponding selected area electron diffraction (SAED) pattern shown in the inset of Fig. 2b reveal that $Zn_{0.9}Co_{0.1}O$ flakes are highly crystalline, showing their wurtzite structure in agreement with the XRD results.

Fig. 3 shows optical absorbance spectra of ZnO and $Zn_{1-x}Co_xO$ flakes. Compared to the spectrum of ZnO, the band edge of the Co-doped ZnO samples is shifted to the lower energy side. The red-shift of the band gap E_g edge with increasing Co concentration into ZnO has been observed [18,19] and interpreted as mainly due to the sp–d exchange interactions between the band electrons and the localized d electrons of the Co^{2+} ions substituting Zn ions [19,20]. The s–d and p–d exchange interactions lead to a negative and a positive correction to the conduction band and the valence band edges, resulting in a band gap narrowing [21]. In addition, with increasing Co concentration up to 0.08, three absorption peaks were also observed around 570, 610 and 660 nm wavelength, which are indicated by arrows in Fig. 3, respectively. These peaks are related to the d–d transitions of the tetrahedrally coordinated Co^{2+} ions and attributed to the $^4A_2(F) \rightarrow {}^2E(G)$, $^4A_2(F) \rightarrow {}^4T_1(P)$, and $^4A_2(F) \rightarrow {}^2A_1(G)$, respectively [22]. The UV–vis spectra give another strong evidence for the partial substitution of Zn^{2+} cations by Co^{2+} in tetrahedral sites of the wurtzite structure.

In order to check the insertion of Co ions into the ZnO lattice and due to the limited sensitivity of the XRD technique, Raman scattering experiments were carried out at room temperature. The room

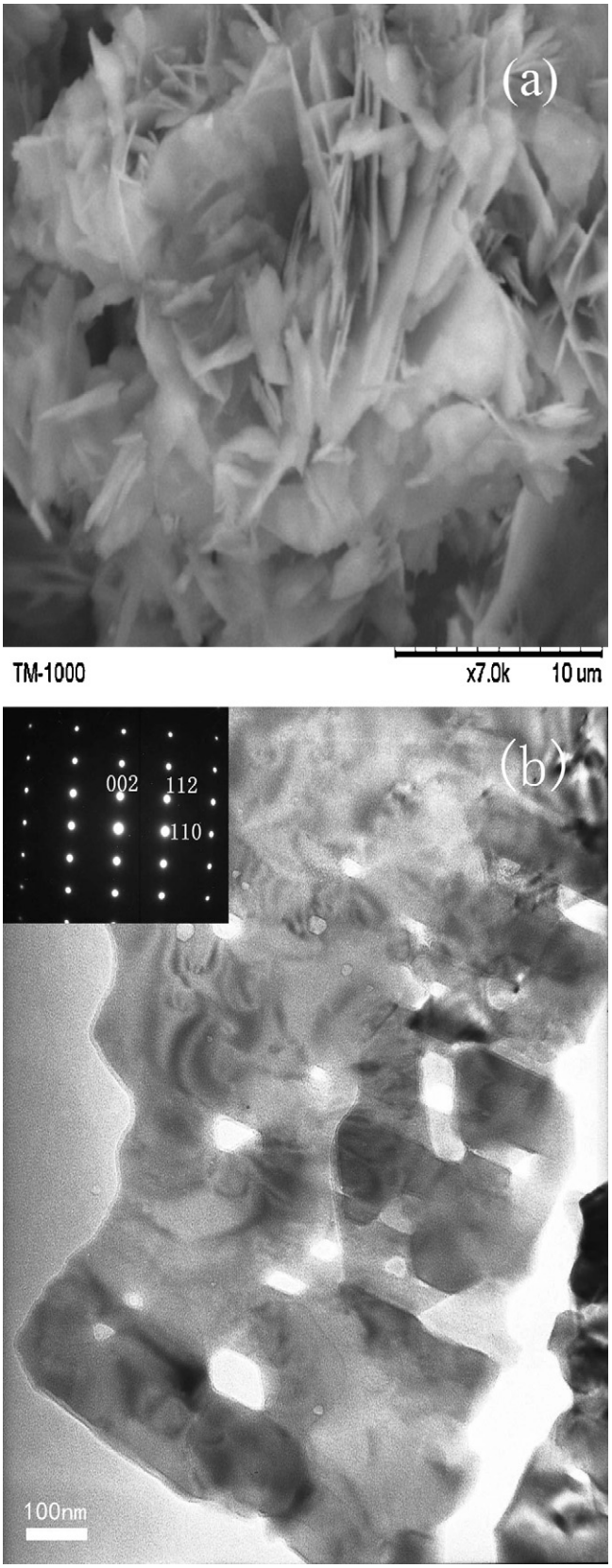

Fig. 2. SEM (a) and TEM (b) images of $Zn_{0.9}Co_{0.1}O$ crystallinity of the flakes. The inset of (b) is an electron diffraction pattern which indicates high crystallinity of the nanocrystals.

Table 1
The lattice constants calculated from the XRD data of $Zn_{1-x}Co_xO$ ($x \leq 0.15$).

$Zn_{1-x}Co_xO$		$x=0$	$x=0.03$	$x=0.08$	$x=0.10$	$x=0.15$
Lattice constant (Å)	a	3.252 ± 0.001	3.237 ± 0.006	3.242 ± 0.004	3.239 ± 0.001	3.242 ± 0.003
	c	5.212 ± 0.003	5.187 ± 0.009	5.194 ± 0.006	5.189 ± 0.001	5.193 ± 0.006

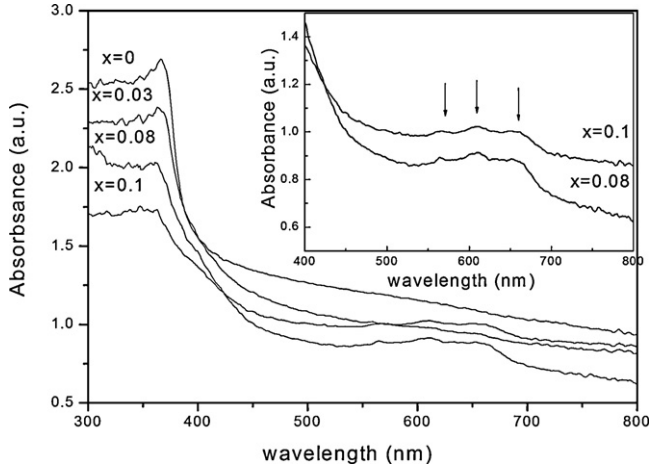

Fig. 3. UV–vis spectra of undoped and doped $Zn_{1-x}Co_xO$ flakes.

temperature Raman spectra of the undoped ZnO and $Zn_{1-x}Co_xO$ ($x \leq 0.10$) samples ranging from 100 to 800 cm^{-1} are shown in Fig. 4. The sharpest and strongest peak around 437 cm^{-1} can be assigned to the nonpolar optical phonon E_2 (high) mode of ZnO. It is related to the motion of oxygen atoms and is a typical Raman active branch of wurtzite ZnO [23,24]. The presence of the E_2 (high) mode in all the three samples indicates the hexagonal wurtzite structure, which is in consistence with the TEM and XRD observations. The peaks at 330 and 379 cm^{-1} are assigned to the second-order vibration mode and the A_1 (TO) mode, respectively. In comparison to the Raman spectrum of undoped ZnO, the mode of AM_1 centered at 540 cm^{-1} can be assigned to the quasi-LO phonon mode due to the abundant shallow donor defects, such as oxygen vacancies or zinc interstitials bounded on the tetrahedral Co sites [25]. The existence of this mode manifests the incorporation of Co in the ZnO lattice. In addition, with increasing Co concentration, there appears a little peak located at about 484 cm^{-1}. The similar peak (475 cm^{-1}) was also observed in Co^{2+} doped, Li^+ and Na^+ codoped, and Co^{2+} and Al^{3+} codoped ZnO and this vibration was not specific to the dopant and its intensity increased by adding doping contents [26,27].

The magnetic properties of the flakes were measured at room temperature. As shown in Fig. 5, the hysteresis (M–H) loops of $Zn_{1-x}Co_xO$ ($x = 0.03$, 0.08, 0.1) exhibited obvious ferromagnetic characteristics. The coercive fields (Hc) are 72.47 ± 0.06, 106.78 ± 0.28 and 73.65 ± 0.15 Oe (see the insets) for $x = 0.03$, 0.08 and 0.1, respectively. The coercive field (H_c) first increases and then decreases with increasing Co concentration. This is similar to the results reported by Diaconu et al. [28]. Saturation magnetization of 0.0118 and 0.0082 emu/g can be observed for $x = 0.03$, 0.08, respectively. When Co concentration is raised to 0.1, hysteresis loop does not show maximum saturation magnetization (Ms). However, no hysteresis loop was observed in the M–H curves of $Zn_{0.85}Co_{0.15}O$ (not shown here). This result may be caused by the enhanced antiferromagnetic coupling between Co ions.

Regarding the possible origin of ferromagnetism in $Zn_{1-x}Co_xO$ ($x \leq 0.1$), the formation of secondary phase such as Co-metal clusters or Co-oxide precipitates should be considered. Concerning Co-related materials, only Co-metal exhibits high-temperature ferromagnetism with T_c of 1400 K [29,30]. While, in the present work, metallic Co is an unlikely source of ferromagnetism because the synthesis of $Zn_{1-x}Co_xO$ samples is performed in air where metallic Co is unable to form. Since there are no Co-related impurities contributing to the room temperature ferromagnetism in the $Zn_{1-x}Co_xO$ flakes, we believe that the observed ferromagnetism at room temperature is an intrinsic property of Co-doped ZnO flakes. The carrier-induced ferromagnetism [12,31,32] that is frequently reported in II–IV semiconductors as well as III–V semiconductor can be the other possible origin of ferromagnetism. In this mechanism, the free carrier concentration is vital to determine whether the material is paramagnetic or ferromagnetic. According to Kittilstved et al. [9], as the Co concentration increases, the free carriers should decrease and Co atoms come close to each other, which imply the presence of some Co^{2+} ions with Co^{2+} nearest neighbors. The superexchange interactions between these neighboring Co^{2+} ions are antiferromagnetic. Therefore, increasing Co concentration will increase the volume fraction of Co^{2+} ions with Co^{2+} nearest

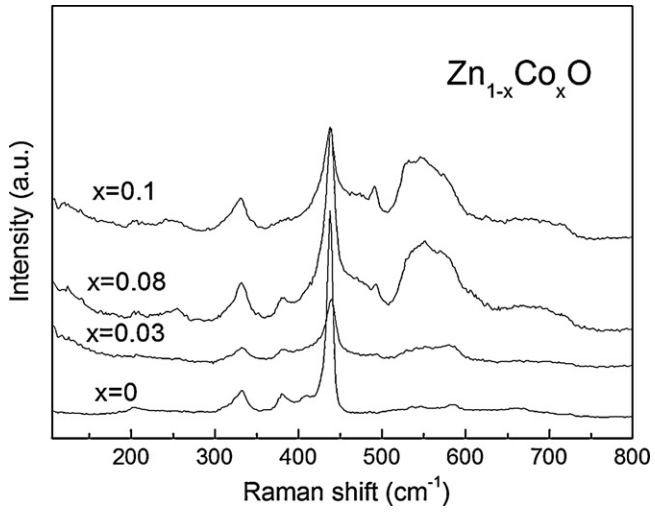

Fig. 4. Room temperature Raman spectra of the $Zn_{1-x}Co_xO$ ($x = 0$, 0.03, 0.08, 0.1) flakes.

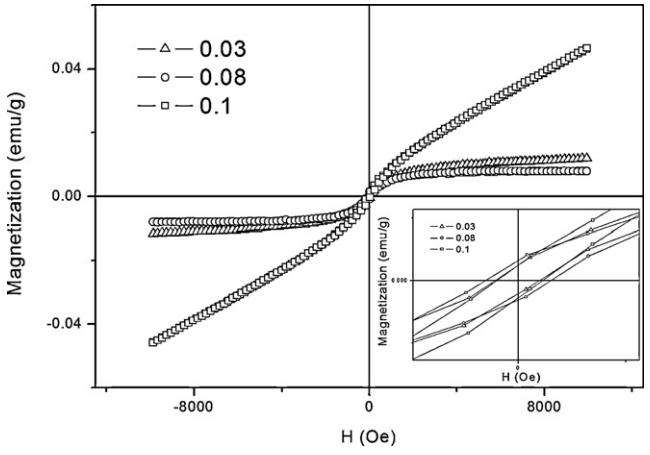

Fig. 5. Magnetization of $Zn_{1-x}Co_xO$ ($x = 0.03$, 0.08, 0.1) as a function of applied field measured at room temperature. The inset shows the zoom-in hysteresis loops.

neighbors. As a result, the enhanced antiferromagnetic interaction suppresses ferromagnetic coupling. Besides, when Co^{2+} concentration x reaches 0.15, Co_3O_4 phase forms, which contributes to antiferromagnetism. So the ferromagnetism in ZnCoO system is suppressed, and then a large paramagnetic effect is observed. The reduction in ferromagnetism with increasing doping concentration is similar to the result of Co-doped ZnO nanorods reported by Yang et al. [33].

4. Conclusions

In summary, we have synthesized the $Zn_{1-x}Co_xO$ flakes though hydrothermal route. Structural analysis indicate that the $Zn_{1-x}Co_xO$ flakes are highly crystalline with wurtzite structure, and no other secondary phase was found at $x \leq 0.1$, which shows the doped Co^{2+} cations are substituted at the Zn^{2+} sites. The M–H curves taken at room temperature indicate that they have obvious ferromagnetic characteristics. The decrease in ferromagnetism with increasing Co concentration demonstrates that ferromagnetism observed at room temperature is an intrinsic property of $Zn_{1-x}Co_xO$ flakes.

Acknowledgments

This work was supported by National Natural Science Foundation of China (Grants 20471007 and 10204003).

References

[1] S.A. Wolf, D.D. Awschalom, R.A. Buhrman, J.M. Daughton, S. von Molnar, M.L. Roukes, A.Y. Chtchelkanova, D. Treger, Science 294 (2001) 1488–1495.
[2] H. Ohno, Science 281 (1998) 951–956.
[3] T. Dietl, H. Ohno, F. Matsukura, J. Cibert, D. Ferrand, Science 287 (2000) 1019–1022.
[4] M. Bouloudenine, N. Viart, S. Colis, A. Dinia, Catal. Today 113 (2006) 240–244.
[5] C. Rath, S. Singh, P. Mallick, D. Pandey, N.P. Lalla, N.C. Mishra, Indian J. Phys. 83 (4) (2009) 415–421.
[6] M.A. White, S.T. Ochsenbein, D.R. Gamelin, Chem. Mater. 20 (2008) 7107–7116.
[7] Y. Kalyana Lakshmi, K. Srinivas, B. Sreedhar, M. Manivel Raja, M. Vithal, P. Venugopal Reddy, Mater. Chem. Phys. 113 (2009) 749–755.
[8] S. Maensiri, P. Laokul, J. Klinkaewnarong, C. Thomas, Appl. Phys. A 94 (2009) 601–606.
[9] K.R. Kittilstved, N.S. Norberg, D.R. Gamelin, Phys. Rev. Lett. 94 (2005), pp. 147209-1–1147209-4.
[10] D. Rubi, J. Fontcuberta, A. Calleja, L. Aragones, X.G. Capdevila, M. Segarra, Phys. Rev. B 75 (2007) 155322.
[11] Y.C. Qiu, W. Chen, S.H. Yang, B. Zhang, X.X. Zhang, Y.C. Zhong, K.S. Wong, Cryst. Growth Des. 10 (2010) 177–183.
[12] Z.L. Lu, W. Miao, W.Q. Zou, M.X. Xu, F.M. Zhang, J. Alloys Compd. 494 (2010) 392–395.
[13] X.J. Liu, X.Y. Zhu, J.T. Luo, F. Zeng, F. Pan, J. Alloys Compd. 482 (2009) 224–228.
[14] Y. Wang, L. Sun, L.G. Kong, J.F. Kang, X. Zhang, R. Han, J. Alloys Compd. 423 (2006) 256–259.
[15] Z.L. Lu, X.F. Bian, W.Q. Zou, M.X. Xu, F.M. Zhang, J. Alloys Compd. 492 (2010) 31–34.
[16] Y.Z. You, T. Fukumura, Z. Jin, K. Hasegawa, M.K. awasaki, P. Ahmet, T. Chikyow, H. Koinuma, J. Appl. Phys. 90 (2001) 4246–4250.
[17] R.D. Shannon, Acta Crystallogr. A 32 (1976) 751–756.
[18] M. Bouloudenine, N. Viart, S. Colis, A. Dinia, Chem. Phys. Lett. 397 (2004) 73–76.
[19] K.J. Kim, Y.R. Park, Appl. Phys. Lett. 81 (2002) 1420–1422.
[20] Y.D. Kim, S.L. Cooper, M.V. Klein, B.T. Jonker, Phys. Rev. B 49 (1994) 1732–1742.
[21] P. Koidl, Phys. Rev. B 15 (1977) 2493–2496.
[22] S. Ramachandran, A. Tiwari, J. Narayan, Appl. Phys. Lett. 84 (2004) 5255–5257.
[23] B.Q. Cao, W.P. Cai, H.B. Zeng, G.T. Duan, J. Appl. Phys. 99 (2006) 073516.
[24] J.B. Wang, G.J. Huang, X.L. Zhong, L.Z. Sun, Y.C. Zhou, E.H. Liu, Appl. Phys. Lett. 88 (2006) 252502.
[25] X. Wang, J. Xu, X. Yu, K. Xue, J. Yu, X. Zhao, Appl. Phys. Lett. 91 (2007) 031908.
[26] J. Alaria, H. Bieber, S. Colis, G. Schmerber, A. Dinia, Appl. Phys. Lett. 88 (2006) 112503.
[27] D. Chu, Y.-P. Zeng, D.L. Jiang, J. Phys. Chem. C 111 (2007) 5893–5897.
[28] M. Diaconu, H. Schmidt, H. Hochmuth, M. Lorenz, G. Benndorf, J. Lenzner, D. Spemann, A. Setzer, K.W. Nielsen, P. Esquinazi, M. Grundmann, Thin Solid Films 486 (2005) 117–121.
[29] J.H. Kim, H. Kim, D. Kim, Y.E. Ihm, J. Appl. Phys. 92 (2002) 6066–6071.
[30] S. Kolesnik, B. Dabrowski, J. Mais, J. Appl. Phys. 95 (2004) 2582–2586.
[31] K. Sato, H.K. Yoshida, Jpn. J. Appl. Phys. 39 (2000) L555–L558.
[32] H.T. Lin, T.S. Chin, J.C. Shih, Appl. Phys. Lett. 85 (2004) 621–623.
[33] L.W. Yang, X.L. Wu, T. Qiu, J. Appl. Phys. 99 (2006) 074303.